Title: Nonlinear Frequency Doubling Up-conversion in Sulfide Minerals Enables Deep-sea Oxygenic Photosynthesis

Authors: Yan Li[1,2]†*, Jiaqi Zhu[1,2]†, Qi Li[3]†, Hao Hong[4]†, Tao Li[3]*, Haoning Jia[1,2], Bingxu Hou[1,2], Houze Lu[1,2], Yanzhang Li[1,2], Jin Xie[4,5], Fuchen Wang[3], Huan Ye[1,2], Kaihui Liu[4,5]*, Anhuai Lu[1,2]*, Jindong Zhao[3,6]*

Affiliations:

[1] SKLab-DeepMinE, MOEKLab-OBCE, School of Earth and Space Sciences, Peking University, Beijing 100871, China.

[2] Beijing Key Laboratory of Mineral Environmental Function, School of Earth and Space Sciences, Peking University, Beijing 100871, China.

[3] Key Laboratory of Algal Biology, Institute of Hydrobiology, Chinese Academy of Sciences, Wuhan 430072, China.

[4] State Key Laboratory for Mesoscopic Physics, Frontiers Science Centre for Nano-optoelectronics, School of Physics, Peking University, Beijing 100871, China.

[5] International Centre for Quantum Materials, Collaborative Innovation Centre of Quantum Matter, Peking University, Beijing 100871, China.

[6] State Key Laboratory of Gene Function and Modulation Research, School of Life Sciences, Peking University, Beijing 100871, China.

†These authors contributed equally to this work.

*Corresponding authors. Email: liyan-pku@pku.edu.cn, litao@ihb.ac.cn, khliu@pku.edu.cn, ahlu@pku.edu.cn, jzhao@pku.edu.cn.

Abstract:

Visible light emission exceeding purely thermal radiation has been imaged at deep-sea hydrothermal vents, yet the underlying mechanisms remain unexplained. Here, we show that visible light can be produced from geothermal infrared radiation via nonlinear frequency-doubling up-conversion in sulfide minerals that are abundant in hydrothermal vents. Chalcopyrite exhibits significant second harmonic generation, which is further amplified under high pressure, yielding a 400–700 nm photon flux three orders of magnitude greater than blackbody emission. When exposure to 1064 nm irradiation, chalcopyrite induces fluorescence responses in the cyanobacterium *Synechococcus* sp. PCC 7002 at 656 and 685 nm, suggesting that the up-converted 532 nm light is absorbed by phycobilisomes and transferred to photosystem II. Metagenomic analysis reveals a strong correlation between cyanobacteria and high-temperature, chalcopyrite-rich vents. Similar up-conversion processes have also been observed in other sulfide minerals, emitting wavelengths covering the entire visible spectrum. These findings unveil a novel mineral-mediated photonic mechanism that generates biologically relevant visible light at hydrothermal vents, which can be harnessed by oxygenic photosynthetic cyanobacteria in Earth's deep biosphere and possibly beyond.

Keywords: second harmonic generation, sulfide mineral, chalcopyrite, deep-sea hydrothermal system, oxygenic photosynthesis, cyanobacteria

INTRODUCTION

Photosynthesis has fueled primary production on Earth for an estimated 3.3~3.4 billion years, continuously shaping the planet surface [1,2]. Surprisingly, photosynthetic prokaryotes like cyanobacteria have also been discovered in deep sulfide deposits associated with both modern submarine hydrothermal vents [3,4] and ancient hydrothermal activity zones [5]. These findings challenge the conventional understanding that oxygenic photosynthesis is impossible in deep hydrothermal systems that are extremely deficient in visible photon fluxes. Despite recent advances on the tolerance of photosynthetic microorganisms to hydrothermal extreme environmental factors, such as high temperatures, low light flux and exposure to metal sulfides [6-8], the long-term survival of photosynthetic cyanobacteria in such deep-earth environments remains a mystery.

The high-temperature upwelling fluids (up to 400°C) in hydrothermal vents not only bring abundant reductants (e.g., H_2S, Fe^{2+}) [9], but also, importantly, emit geothermal radiation [10-14]. Some anaerobic photosynthetic bacteria have been shown to survive through harvesting low-energy photons from the weak red and near-infrared spectrum of this geothermal radiation [7,8]. For instance, a green sulfur bacterium isolated from a hydrothermal vent in the East Pacific Rise area employs bacteriochlorophyll *c* (BChl *c*) to absorb and utilize red/infrared light [8]. However, the survival of oxygenic photosynthetic cyanobacteria in hydrothermal vents [3,4] poses greater challenges due to the requirement for higher-energy photons (wavelength of 390–750 nm). According to blackbody radiation principles, photon emission in the visible light range from the hydrothermal vents is significantly limited [11-14].

Previous *in situ* underwater spectral cameras have recorded a remarkable photon flux of visible light (400–600 nm) around hydrothermal vents, reaching 10^4 photons·cm^{-2}·s^{-1}·sr^{-1}, which exceeds the upper limit of the thermal blackbody radiation (10^3 photons·cm^{-2}·s^{-1}·sr^{-1}) [13,14]. The actual photon fluxes may be even higher, given the signal attenuation caused by light scattering over measurement distances [12] and data

processing losses during image flat-fielding correction and noise elimination [13,14]. The origin of this excess visible light remains unresolved. Proposed hypotheses, including crystalloluminescence [15] and triboluminescence [16], are typically associated with the presence of sugars or copper sulfate, while chemiluminescence [17] can only be efficient when induced by rapid oxidation of sulfides in aerobic environments. Although vapor bubble luminescence [18] can rapidly generate intense flashes, its transient and intermittent nature precludes the sustained and stable photon flux necessary for photosynthesis.

Here, we present experimental evidence that sulfide minerals in hydrothermal vents exhibit an infrared-to-visible photon up-conversion property, which is greatly enhanced by pressure and can provide sustainable visible photons for cyanobacterial photosynthesis in deep-sea hydrothermal vents. This unique mineralogical mechanism of visible light generation provides insights into cyanobacterial growth in deep hydrothermal systems, and has implications for the origin, evolution, and even the current occurrence of oxygenic photosynthesis on Earth and other water worlds in the solar system.

RESULTS AND DISCUSSION

Characterization of second harmonic generation (SHG) in natural sulfides

Spectroscopic measurements were performed on sulfide minerals from high-temperature hydrothermal vents to explore their luminescent characteristics (Fig. 1). The sulfide samples were collected from the Longqi hydrothermal vent field in the southwest Indian ridge. Their phases, as identified by XRD (Fig. S1), mainly comprised chalcopyrite ($CuFeS_2$), sphalerite (ZnS), pyrite (FeS_2) and pyrrhotite ($Fe_{1-x}S$, $x<1$) with mass percentages of 54%, 26%, 15% and 5%, respectively. Considering that hydrothermal vents mainly emit thermal radiation within the infrared spectrum, we used a wide-band infrared light (800–1500 nm) to excite the sulfide minerals (Fig. 1b). The emission spectra revealed that chalcopyrite exhibited detectable light emissions in the range of 420–540 nm, with an emission peak at ~471 nm (Fig. 1b).

The maximum emission peak remained unchanged under different excitation light powers (Fig. S2). In contrast, the other four sulfide minerals exhibited no discernible visible light emissions. The spectral overlap between chalcopyrite SHG emission and the excess photon flux (400–550 nm) observed at hydrothermal vents suggests that chalcopyrite is a desired candidate for efficiently upconverting infrared to visible light in deep-sea environments.

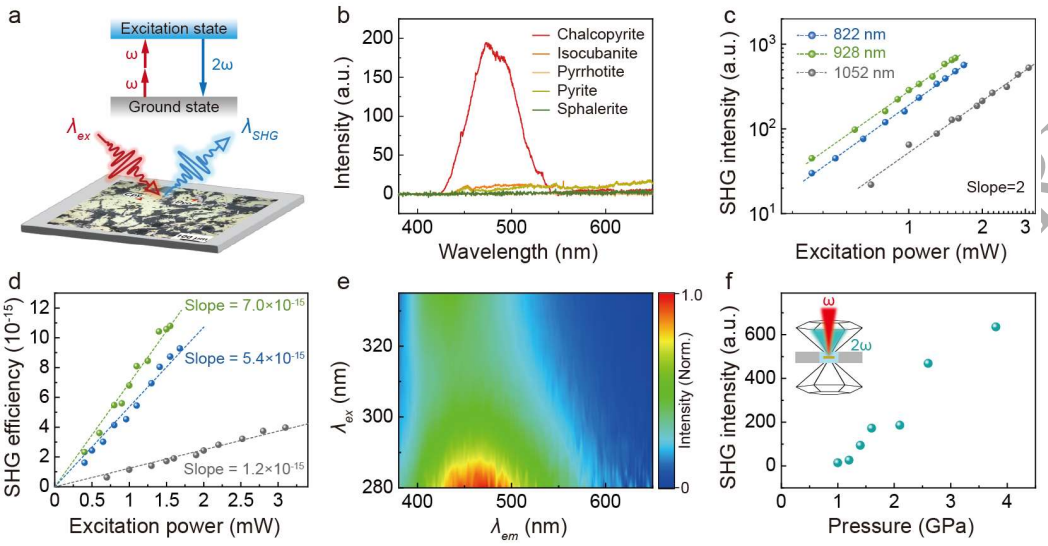

Figure 1. Optical spectrum analysis of chalcopyrite from deep-sea hydrothermal vents. (a) Schematic diagram of frequency-doubling measurement on the deep-sea hydrothermal sulfides. Two photons at the frequency ω interact with the sulfide sample and generate a new photon with a doubled frequency (2ω) and half the wavelength of the excitation light. (b) Emission spectra of sulfide minerals under a supercontinuum laser (800–1500 nm). Compared to the other four sulfides, the spectrum of chalcopyrite shows an obvious peak at ~471 nm. (c) Excitation power-dependent second harmonic generation (SHG) intensity in chalcopyrite. Under different excitation wavelength, all three curves show the expected quadratic law. (d) Excitation power-dependent frequency-doubling conversion efficiency in chalcopyrite. The conversion efficiency increases linearly with the excitation light power, arriving over ~10^{-14} at 1.5 mW with 928 nm excitation. (e) Two-dimensional photoluminescence spectrum of chalcopyrite showing a peak at ~471 nm, consistent with that from SHG spectrum in (c), indicating a special excitation state at ~2.63 eV. (f) Emission spectra of chalcopyrite measured in a diamond anvil cell (DAC), showing increasing SHG intensity with hydrostatic pressure.

To study the infrared-to-visible photon up-conversion mechanism of chalcopyrite, we measured the emission spectra under three monochromatic light (822, 928 and 1052

nm) and at different excitation powers (0.45–3.20 mW). The emission peak was exactly centered at half of excitation wavelength (411, 464 and 526 nm) and remained unchanged with increasing excitation power (Fig. S3). The double-frequency emission intensity of chalcopyrite exhibited a quadratic correlation with the excitation power (Fig. S4), as supported by fitting slope values of 2 in the logarithmic coordinate view (Fig. 1c). The frequency-doubling conversion and the quadratic relationship indicated that the up-conversion mechanism was attributed to SHG effect [19]. In brief, two photons with frequency ω excited chalcopyrite from the ground state to an excited state, resulting in emission of a new photon with twice the energy of the initial photon (i.e., double the frequency and half the wavelength, shown as Fig. 1a). Based on the emission spectra under three monochromatic lights, we calculated the energy conversion efficiency (η) of chalcopyrite at varying excitation power (P_{ex}) and derived linear relationships between η and P_{ex} (Fig. 1d). As P_{ex} gradually increased from 0.4 to 1.5 mW, η increased from 10^{-15} to 10^{-14}. Notably, the SHG efficiency of chalcopyrite is strongly dependent on the excitation wavelength, as illustrated by diverging linear fitting slopes (Fig. 1d).

To further explore the excitation wavelength-dependent SHG effect in chalcopyrite, we measured the photoluminescence (Fig. 1e) spectra of chalcopyrite to probe the electronic transitions between the specific excitation and ground states. The two-dimensional photoluminescence spectrum showed that under ultraviolet light excitation (λ_{ex} = 280–340 nm), chalcopyrite exhibited an intense and fixed emission in the range of 420–500 nm (λ_{em}), peaking at ~471 nm (Fig. 1e). This peak position was in accordance with the SHG emission peak position presented in Fig. 1c, indicating the existence of an energy gap at ~2.63 eV (corresponding to a photon wavelength of 471 nm) between the excited state and the ground state of chalcopyrite. Upon irradiation at 928 nm, approximately double the wavelength of 471 nm, chalcopyrite underwent resonant excitation that maximized the upconverting efficiency at the energy gap, thereby producing a strong SHG emission at 471 nm. This up-conversion mechanism is distinct from fluorescence or down-conversion luminescence

mechanisms (e.g., rare-earth element luminescence) [20,21] previously found in minerals. It enables chalcopyrite to constantly convert geothermal infrared radiation into visible light when exposed to a thermal radiation field.

Pressure-enhanced SHG effect in chalcopyrite

Notably, the deep-sea environment is characterized by a high-pressure condition. To understand the relationship between the SHG efficiency of chalcopyrite and the hydrostatic pressure, pressure experimental simulation was performed in a diamond anvil cell (DAC). The results indicated a significant increase in the up-conversion efficiency of chalcopyrite from infrared to visible light under high hydrostatic pressure, with the maximum efficiency reaching up to 10^{-7}, which is 66 times higher than its initial value (Fig. 1f). The enhanced SHG effect under pressure can be explained by the Miller's rule, where the increased material density and refractive index under pressure contribute to an augmented nonlinear susceptibility [22]. Additionally, the cation displacement within the mineral lattice and the evolved band structure with increasing pressure further contribute to the enhancement of SHG (Fig. S5) [23]. This implies that the flux of visible photons converted by chalcopyrite could be substantially enhanced under actual deep high-pressure environments, such as deep hydrothermal vents.

According to the blackbody curve, the photon flux of hydrothermal vents at 400°C is approximately on the order of 10^{12} photons·cm^{-2}·s^{-1}·sr^{-1} in the 800–1100 nm range. Considering the pressure effect, the photon fluxes in the 400–550 nm range generated by the SHG effect of chalcopyrite (with maximum efficiency up to 10^{-7}) could reach 6.6×10^{6} photons·cm^{-2}·s^{-1}·sr^{-1}, three orders of magnitude greater than the blackbody radiation [11-14]. Previous research on the self-focusing effect induced by thermal gradients suggests that localized photon flux could be further enhanced through mineral micropores in the steep temperature gradient field of hydrothermal vents [24]. Therefore, the pressure-enhanced SHG effect in chalcopyrite could significantly contribute to the anomalously high blue-green visible photon flux observed at

hydrothermal vents.

Fluorescence response of cyanobacteria to infrared-irradiated chalcopyrite

Cyanobacterial pigments efficiently absorb visible light within the 400–710 nm range [25]. While the majority of excitation energy transferred to PSII from PBS is used to drive electron transport for oxygen evolution, it can also produce fluorescence through a relaxation process [26]. To investigate if an infrared light can be used to excite PSII, the cyanobacterium *Synechococcus* sp. PCC 7002 (*Synechococcus* 7002) was placed on a chalcopyrite substrate and *in-situ* measurement of its fluorescence response to infrared light was performed (Fig. 2a).

Upon excitation by a 1064 nm monochromatic light (P_{ex}=13 mW), we observed a sharp peak at 532 nm and a broad peak ranging from 610 to 810 nm in the emission spectrum (Fig. 2b). When chalcopyrite was replaced by a glass substrate or galena (PbS, with similar reflectivity and thermal conductivity to chalcopyrite), no significant fluorescence emission was recorded (Fig. 2d), contrasting sharply with the chalcopyrite substrate (Fig. 2c). If *Synechococcus* 7002 was replaced with a sterile culture medium (A-plus), the broad emission peak was not detected (Fig. 2d). Thus, the 532 nm peak corresponds to the SHG emission in chalcopyrite, while the broad emission peak comes from the cyanobacterial cells.

The cyanobacterial fluorescence spectrum can be fitted with three component peaks at 656, 685 and 713 nm (Fig. 2c). The peaks at 656 and 685 nm indicate that the up-converted light by chalcopyrite is successfully absorbed by PBS and the excitation energy is transferred to PSII [27,28]. Despite the partial overlap between the two peaks within 680–800 nm range, the component peak at 713 nm aligns with the characteristic fluorescence emission wavelength of PSI in *Synechococcus* 7002 [29,30]. This observation suggests that excitation energy can be transferred to PSI, consistent with recent studies on interactions between rod-shaped phycobilisomes and PSI [31,32]. Distinct from Chl *d*/*f*-dominated infrared absorption supporting PSI

centric cyclic electron transport (P700 → P700*), mineral-upconverted visible light can directly provide higher-energy photons to drive PSII charge separation and electron transport for oxygen-evolving reaction [33].

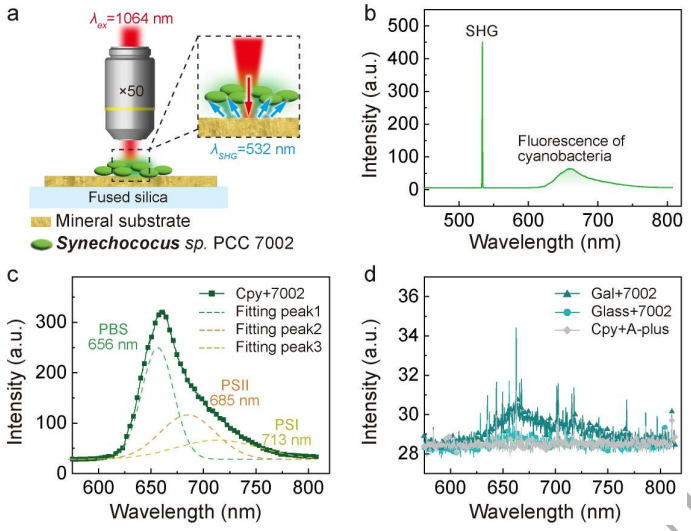

Figure 2. Fluorescence response of cyanobacteria to infrared-irradiated sulfide minerals. (a) Schematic diagram of the fluorescence experiments. The wavelength of excitation laser (λ_{ex}) and the wavelength of SHG (λ_{ex}) is 1064 and 532 nm, respectively. The magnification of objective lens is denoted as ×50. (b) Emission spectrum of *Synechococcus sp.* PCC 7002 (*Synechococcus* 7002) upon a chalcopyrite substrate irradiated by 1064 nm infrared light. (c) Fluorescence spectra of *Synechococcus* 7002 recorded on chalcopyrite (Cpy, forest green curve with square). The fluorescence emission from *Synechococcus* 7002 on Cpy can be well fitted with three component peaks at 656, 685 and 713 nm, indicative of the up-converted light is absorbed by phycobilisome (PBS, fitting peak1, bright green dashed curve) and the excitation energy is transferred to photosystem II (PSII, fitting peak2, orange dashed curve) and photosystem I (PSI, olive yellow dashed curve). (d) Fluorescence spectra of *Synechococcus* 7002 recorded on glass (Glass, cyan curve with circle) and galena (Gal, dark cyan curve with triangle). No detectable fluorescence was observed when substituting Cpy with a glass or Gal substrate, or replacing *Synechococcus* 7002 with a sterile culture medium (A-plus, grey curve with diamond).

Close correlation of deep cyanobacteria with high-temperature vents revealed by metagenomics

Since no successful isolation and culture of oxygenic photosynthetic microorganisms from deep-sea hydrothermal systems have been reported, assessing the completeness

of photosynthetic functional genes appears to be an ingenious suboptimal approach for investigating the potential presence of oxygenic photosynthetic bacteria in the deep sea. A total of 142 sets of metagenomic data were collected from 19 global hydrothermal vents and 24 deep-sea locations distant from hydrothermal vents to analyze photosynthesis-related genes. These datasets were classified into four types based on their mineral components, geographical locations and temperature ranges (Fig. 3b): hydrothermal vents with a central temperature above 350°C are denoted as Type C1, enriched in Cu- and Fe-sulfide minerals like chalcopyrite, isocubanite, pyrrhotite; hydrothermal vents with a central temperature below 350°C are denoted as Type C2, generally enriched in Pb- and Zn-sulfide minerals like sphalerite and galena; shallow-water hydrothermal deposits in the epipelagic zone are denoted as Type S; and deep-sea locations distant from hydrothermal vents are denoted as Type N [34,35]. The photosynthesis genes analyzed in this metagenomic comparison include those encoding proteins of photosystem I (PSI), photosystem II (PSII), cytochrome b_6f complex (Cytb_6f), photosynthetic electron transport, F-type ATPase and phycobilisomes (PBS), which function as light-harvesting antennas (Fig. 3a and Fig. S6).

The completeness of genes encoding each phototrophic apparatus in all metagenomic datasets is presented in Fig. 3b, including 27 datasets from Type C1, 43 datasets from Type C2, 30 datasets from Type S, and 30 randomly selected datasets from Type N (out of 42 available). A comprehensive metagenomic analysis of photosynthesis-related genes in all datasets is illustrated in Fig. S6. Notably, 10 out of the 27 datasets from Type C1 (C1_9-18) exhibit a high degree of completeness in genes associated with phototrophic apparatuses. In these datasets, the genes encoding PSI, PSII, Cytb_6f and components of photosynthetic electron transport are nearly complete, with the average completeness of PBS genes approaching 80%. Specifically, these datasets contain a rich array of photosynthetic genes encoding the proteins involved in oxygenic photosynthesis, such as the *psa* and *psb* genes encoding PSI and PSII subunits, respectively. The majority of the *psa* genes including *psaA*, *psaB*, *psaC*,

psaD, *psaE*, *psaF*, *psaI*, *psaJ*, *psaK*, *psaL* and *psaM* are found in these datasets. Moreover, the Type C1 datasets that have *psa* genes simultaneously possess high-abundance *psb* genes encoding PSII subunits, such as PSII reaction center proteins D1, D2, Cytb559, CP47 and CP43 [36]. Among other photosynthetic electron transfer proteins, a complete set of Cytb_6f complex genes are found in these datasets from Type C1. The presence of Cytb_6f small subunit genes and *petH* (plant-type ferredoxin: NADPH oxidoreductase, FNR) is particularly interesting, as they are present only in the oxygenic photosynthetic electron transfer chain.

The datasets from Type C1 with the photosynthetic genes above also possessed a set of *apc*, *cpc*, and *cpe* genes that encode allophycocyanin, phycocyanin and phycoerythrin of PBS, respectively. Notably, cyanobacteria can dynamically adjust PBS components to optimize the selective utilization of specific chromophore types, thereby maximizing the absorbance of the predominant wavelengths in the ambient light spectrum [37]. Geothermal radiation emitted by hydrothermal vents is dominated by infrared light and an excess photon flux in the 400–550 nm range. While far-red-light photoacclimation (FaRLiP) could theoretically facilitate photosynthesis in such environments, metagenomic analysis revealed no FaRLiP-associated genes (*apc*D2, *apc*D3, and *apc*D5) [38-40] in Type C1 samples (Fig. S6), excluding the potential distraction of FaRLiP. This finding suggests that hydrothermal photosynthesis relies on visible light rather than far-red/infrared light.

Metagenomic assembly demonstrated the consistent detection of key cyanobacterial photosynthetic genes (*psaABCD*, *psbABCD*, *apcABC*, *cpcABC*, and *cpeABC*) in vent-associated samples (C1_10-18), while these genes were virtually absent in randomly selected control samples (Fig. S7). These findings are in accordance with the those mentioned previously in this section, thereby collectively reinforcing the presence of cyanobacterial photosynthetic genes at high-temperature mineral-containing hydrothermal vents.

To distinguish between *in situ* activity and passively transported sources, we further

traced the corresponding species for common photosynthetic genes, including *apc*AB, *cpc*AB, *psa*ABC and *psb*ABC (Supplementary Data2). Notably, *Prochlorococcus psb* genes, which are expected in settling biomass due to their marine abundance [41], are absent in the samples with complete oxygenic photosynthetic genes (*psa*, *psb*, *apc*, *cpc*) and electron transport chain components (C1_10/11/12/13/15/16/17). This discrepancy challenges passive settling hypotheses, supporting endogenous cyanobacterial DNA at vents.

Based on the *in-situ* microbial information in datasets from Type C1, we can decode endemic ecological advantages for sustaining complete photosynthetic genes in high-temperature mineral-containing vents, by conducting comparisons with datasets from diverse geographical locations, including Type C2, Type S and Type N. The datasets from Type C2 featuring lower temperature (<350ºC) and different mineral components from Type C1, exhibit a general absence of PSI, PSII and Cytb_6f genes, except for five of 43 datasets (SRR14000033, SRR14000034, SRR7168047, SRR7168048, and SRR7168049). These five datasets, which were obtained from deep-sea locations (>3,000 m) with temperatures around 290ºC, do not contain a complete set of genes encoding the proteins of PBS or some photosynthetic electron transfer chain (*psb*X, *psb*Y, *psb*Z). This suggests that hydrothermal environments with higher central temperature appear to be more favorable for preserving genes encoding light-harvest antenna proteins.

Our analysis further extended to Type S datasets, which contain a relatively complete set of photosynthetic genes, as previously reported [42,43]. By contrast, nearly all genes encoding PBS were absent in Type N datasets, with over 70% of genes encoding PSI and PSII remaining incomplete. These findings further reveal the crucial role of hydrothermal vent-derived geothermal radiation in maintaining complete photosynthetic functional genes in phototrophic microorganisms. Particularly, the cyanobacteria founded in deep subsurface rock have completely lost the fluorescence response of PSII [5]. This is consistent with the results of our metagenomic analysis of the two samples (T1_1/2): half of the genes encoding PSII and almost all the genes

encoding PBS are missing. This loss of key photosynthetic genes is explained as the consequence of long-term heterotrophic adaptation to dark environments [5,44,45]. However, our findings with relatively complete genes encoding oxygenic photosynthesis and light-harvesting antenna proteins imply a more active phototrophic mode at hydrothermal vents.

Notably, certain metabolic strategies may bridge these ecological extremes. For example, some *Synechocystis* species (e.g., PCC 6803) can engage in light-activated heterotrophic growth (LAHG) [46-48], while metagenomic evidence from the active Jabberwocky vent reveals co-occurrence of complete Calvin–Benson–Bassham (CBB) and reductive tricarboxylic acid (rTCA) cycles [4], suggesting metabolic flexibility in these environments. These findings collectively point to hydrothermal vents as unique niches where geothermal radiation sustains phototrophic potential, while fostering diverse energy-capture strategies.

Besides the datasets mentioned above, 19 additional sets of metagenomic data from the oxidation zone of hydrothermal minerals (denoted as O, enriched in Ba- and Ca-sulfate minerals), and thermophilic microbial community after enrichment culture (denoted as T2) were analyzed (Fig. S6). The photosynthetic genes were also observed in datasets from T2, although some *psa* and *psb* genes were not detected. Datasets from Type O exhibited a lower abundance of photosynthetic genes overall. While some datasets contained relatively complete sets of photosynthetic genes, they were almost entirely missing the *apc*, *cpc*, and *cpe* genes that encode phycobiliproteins (Fig. S6).

Since nearly all datasets contained an intact set of *atp* genes encoding F-type ATPase, reads mapped to these genes from various species were utilized to analyze community composition and diversity (Fig. S8). Cyanobacteria were observed in the Type C1 datasets, and the microbial composition of Type C1 showed similarities to that of Type S datasets from the shallow euphotic zone. Comparative analysis of Types C1, C2, and O suggests that vent-specific metal sulfide minerals may create unique

ecological niches favoring oxygenic phototrophs in aphotic depths. While prior metagenomic studies have reported sporadic occurrences of oxygenic phototrophs in hydrothermal systems [3-5], our work provides the first comprehensive genomic evidence for the preservation of complete photosynthetic pathways in high-temperature vent environments.

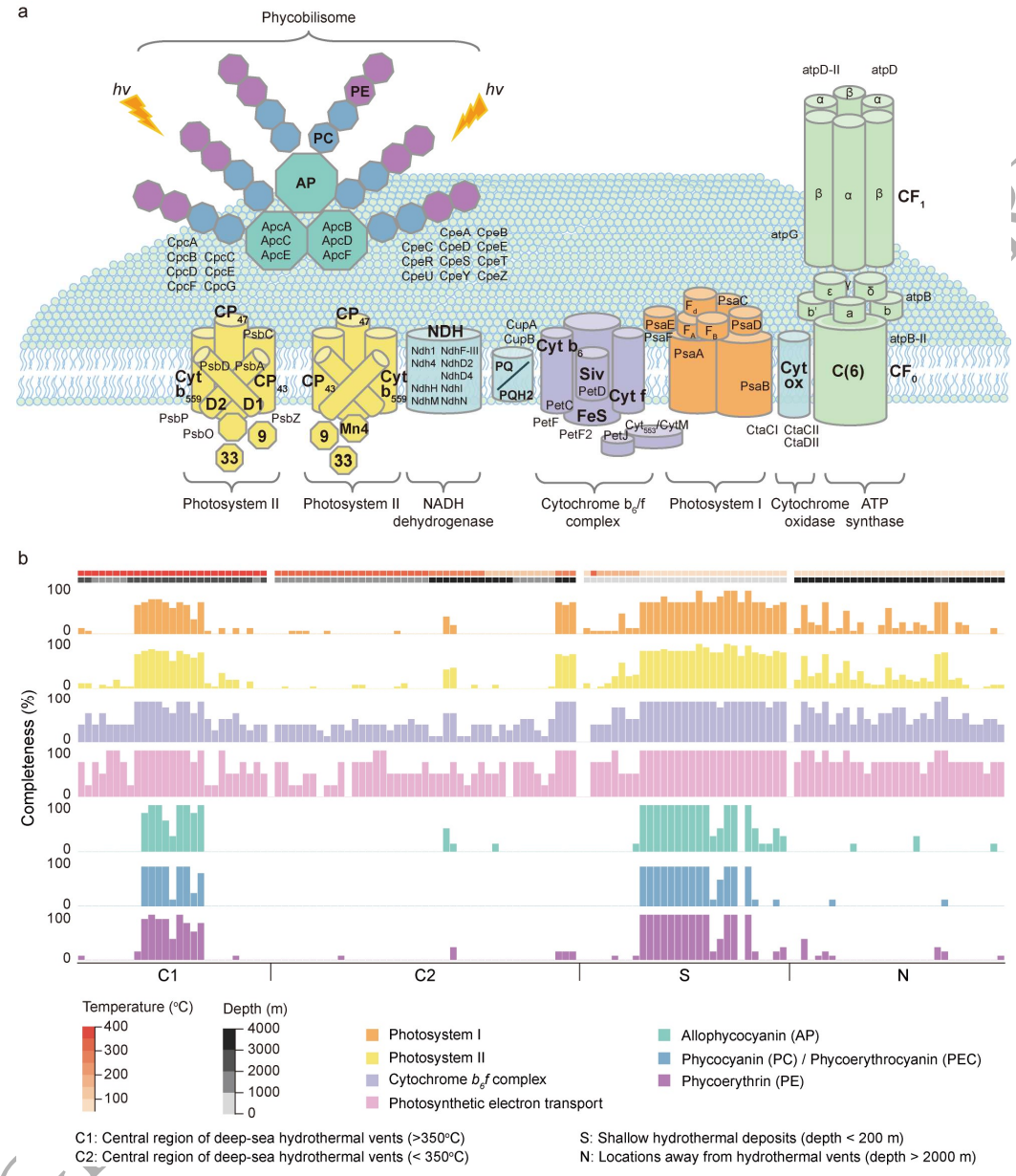

Figure 3. Metagenomic analysis of photosynthesis-related genes in marine systems. (a) Diagram illustrating photosynthetic electron transfer and functional genes associated with the phototrophic apparatus, including Photosystem I, Photosystem II,

Cytochrome b_6f complex, Photosynthetic electron transport, Allophycocyanin (AP), Phycocyanin (PC)/Phycoerythrocycanin (PEC) and Phycoerythrin (PE). (b) Completeness of functional genes related to the phototrophic apparatus of datasets across four marine environments. Metagenomic datasets are classified into: 27 from central region of deep-sea hydrothermal vents (C1, >350°C), 43 from central region of deep-sea hydrothermal vents (C2, <350°C), 30 from shallow hydrothermal deposits (S), and 42 from deep-sea locations distant from hydrothermal vents (N).

Extensive visible emissions in hydrothermal sulfide minerals

We have demonstrated that natural chalcopyrite exhibited a strong SHG effect in the near-infrared region (Fig. 1), with a nonlinear frequency-doubling up-conversion efficiency comparable to those of artificial chalcopyrite-structured materials, such as $AgGaS_2$ [49], $AgGaSe_2$ [49], $ZnGeP_2$ [50]. Theoretically, sulfide minerals with non-centrosymmetric crystal structures, high nonlinear optical coefficients, and suitable electronic band structures [51,52] may exhibit strong nonlinear frequency-doubling up-conversion effects. Given the diversity of hydrothermal sulfide minerals, we investigated the potential of 12 additional sulfide minerals (Fig. S8 and Fig. S10) to upconvert near-infrared light to visible light.

Upon being triggered by 800–1500 nm light, molybdenite (MoS_2), stibnite (Sb_2S_3), bismuthinite (Bi_2S_3) and orpiment (As_2S_3) emitted light within the 420–725 nm range (Fig. 4a). It indicates that besides the superior up-conversion efficiency of chalcopyrite in the blue-green band (Fig. S11), other sulfide minerals could also contribute visible light sources in deep hydrothermal fields through broadening the up-conversion wavelength range. Collectively, their emission wavelengths would cover full range of visible light spectrum from the blue-green band of 400–500 nm to the red band of 600–700 nm. The photon flux generated by SHG from various minerals could provide energy to support oxygenic photosynthesis in deep-sea environments (Fig. 4b) through diverse photosynthetic pigments such as chlorophyll *a*, chlorophyll *b* and carotenoids [53,54]. For example, the SHG emission spectra of chalcopyrite and bismuthinite offer visible light within the range of 400–550 nm, matching the absorption peak of chlorophyll *a* at ~430 nm and that of phycourobilin

at ~495 nm [55]. Molybdenite and stibnite with SHG emission peaks at 570–620 nm can provide visible light for phycoerythrocyanin with an absorption peak at ~575 nm [56]. These multi-sourced visible lights may also benefit other phototrophic bacteria in deep-sea that absorb light in the 450 to 700 nm range.

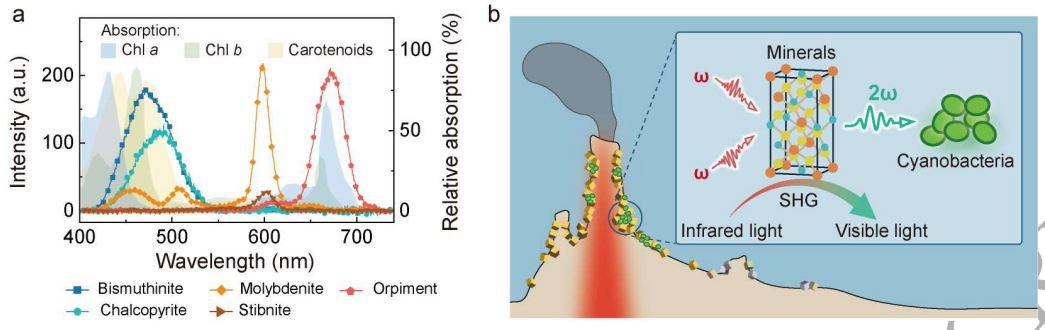

Figure 4. Extensive visible emissions in hydrothermal sulfide minerals. (a) SHG emission spectra of five sulfide minerals overlapping with the absorption spectra of photosynthetic pigments (chlorophyll *a*: blue area, chlorophyll *b*: green area, carotenoids: yellow area). (b) Schematic illustrating the mineralogical mechanism which converts infrared light into visible light via SHG, thereby supporting photosynthetic microorganisms in the deep sea.

Geological implications

Chalcopyrite, as one of the earliest and major sulfide minerals at high-temperature hydrothermal environments, exhibits a strong SHG effect through nonlinear optical processes that convert two infrared photons into a single visible photon with doubled frequency. This frequency-doubling up-conversion phenomenon is predominantly observed in minerals with broken inversion symmetry, such as the hydrothermal sulfide minerals in this study. With pressure-enhanced effect, the chalcopyrite-mediated photon conversion at 400ºC vent can generate visible emission exceeding blackbody radiation values by three orders of magnitude, aligning with the excess blue-green light observed at hydrothermal vents. Additionally, previous studies have demonstrated that the metal sulfides at hydrothermal vents can exist as aggerates of nanoparticles (individual as small as 4 nm) [57,58]. The resonance enhancement resulting from nano-microcavity structure on mineral surface (Fig.S12) and self-focus effect induced by steep thermal gradient can further improve the up-conversion

emission by three orders of magnitude [19,20,24,59]. Based on these findings, we propose that deep hydrothermal sulfide minerals like chalcopyrite provide a significant flux of visible light around the vents by upconverting the abundant geothermal infrared light (Fig. 4b).

The fluorescence experimental evidence from *Synechococcus* 7002 demonstrates efficient energy transfer from mineral-converted visible photons to PBS, subsequently activating both PSII and PSI reaction centers (Fig. 3a). This offers a strong physical basis for understanding the discovery that most oxygenic photosynthetic genes, especially those encoding light-harvesting antenna proteins, are present in deep high-temperature hydrothermal vents. The observed correlation between cyanobacterial DNA and regions with high temperature (>350ºC), high hydrostatic pressure and the occurrence of sulfide minerals suggests endemic ecological niches supporting deep-sea photosynthesis. These findings not only open new pathways for exploring how deep-sea oxygenic photosynthesis functions, but also probes potential geochemical drivers for the evolution of oxygenic photosynthesis.

Cyanobacteria played a pivotal role in the Great Oxidation Event (GOE) at ~2.4 Ga, and their marine expansion is regarded as a key driver for atmospheric O_2 rise and carbon burial [60,61]. Interestingly, the GOE coincided with the breakup of the supercontinent that spurred global magmatic processes and extensive deposition of hydrothermal minerals [62,63]. This deep temporal correlation suggests a possible causal relationship between hydrothermal activities and thriving cyanobacteria. Besides, given the geological hydrothermal activities prior to the GOE and their continuous eruption [63], the mechanism described in our report could also plausibly have contributed to the so-called whiffs of oxygen on early Earth before the GOE [64]. Specifically, with an early Earth's geothermal heat flux two to three times higher than the modern value [65], the visible light flux produced by this up-conversion mechanism in sulfide minerals would have been higher. The abundant microcavities in the actual hydrothermal chimney (Fig. S11) not only can enhance the SHG effect [59], but also provide shelters against intense ultraviolet radiation [66] or the strong

impact of hot fluids or toxic vapors for early oxygenic photosynthetic microorganisms.

Although previous studies have proposed alternative habitat preferences for the origin of early cyanobacteria (e.g., soil/freshwater, low-salinity environments) [67,68], our findings demonstrate that the mineral up-conversion mechanism could have provided a crucial energy source for the parallel evolution, adaptation, and colonization of early oxygenic photosynthetic microorganisms in hydrothermal environments. Our results support the hypothesis that early cyanobacteria might have utilized excess light emission at hydrothermal vents to occupy ecological niches in the deep sea, where they thrived and potentially evolved sophisticated photosynthetic proteins within these deep hydrothermal environments.

While our findings provide a blue-green light source, continuous light stimulation, and selective pressure for photosynthesis at hydrothermal vents, several limitations warrant cautious interpretation. The *in-situ* observed photon flux (>10^4 photons·cm^{-2}·s^{-1}·sr^{-1}) and mineral up-conversion emission evaluated in this work (~10^7 photons·cm^{-2}·s^{-1}·sr^{-1}) exhibits a measurable discrepancy from the photon requirement for cyanobacterial laboratory growth (~10^{13} photons·cm^{-2}·s^{-1}·sr^{-1}). However, emerging evidence suggests that natural phototrophs may operate at lower photon fluxes than laboratory models. For example, Hoppe et al. (2024) demonstrated that oxygenic photosynthesis can persist at photon fluxes as low as 0.04 ± 0.02 μmol photons·m^{-2}·s^{-1} (~10^{11} photons·cm^{-2}·s^{-1}·sr^{-1}), implying the adaptations of natural phototrophs to extreme low-light conditions that remain poorly understood [69]. Consequently, while the lack of *in situ* isolation/cultivation evidence and precise spectral emission measurements at deep-sea environments restrict our capacity to fully resolve this gap, our study establishes minerals' intrinsic photon-generating capacity as a novel mechanism warranting further interdisciplinary investigation.

In summary, our findings on mineral up-conversion potentially contribute to the essential light source for the evolution and operating of oxygenic photosynthesis in Earth's deep hydrothermal vents. This also raises the possibility of discovering new

lineages of photosynthetic microorganisms and even an ecosystem beneath the icy surfaces of other water worlds beyond Earth, such as Europa [70] and Enceladus [71], which potentially host ice-covered oceans supported by live hydrothermal vents. To facilitate future astronomical and astrobiological explorations, we propose establishing a coupled mapping framework of spectral signals between mineral SHG and photosynthetic pigments, providing a novel mineralogical approach for detecting potential photosynthetic life beyond Earth.

METHODS

Optical characterization of minerals

The second harmonic generation (SHG) effects of natural black chimney samples and other sulfide minerals were measured using an incident light source generated from the supercontinuum white light system (WhiteLaser SC400, Fianium) with a basic pulse width of 6 ps and a fundamental frequency of 40 MHz. The conversion efficiency comparison experiment of chalcopyrite ($CuFeS_2$), bismuthinite (Bi_2S_3), stibnite (Sb_2S_3), orpiment (As_2S_3) and molybdenite (MoS_2), were measured using a titanium-sapphire pumped laser (Mira-HP, Coherent) as incident light, with a basic pulse width of ~130 fs and a fundamental frequency of 76 MHz. The SHG spectroscopies were measured by a home-made set-up with a reflective geometry at room temperature (Fig. S13). The spot size of the pumped laser is about 10 μm^2 under focus of a 20× objective (Nikon) and 4 μm^2 under focus of a 50× objective (Nikon). The generated SHG signal was collected by the same objective. After filtering out the excitation laser, SHG signal was recorded using a spectrometer (SP2500, Princeton Instruments) equipped with a nitrogen-cooled silicon charge coupled device (CCD) camera (PyLoN 400 BRX, Princeton Instruments). A monochromatic light signal is obtained by placing a bandpass filter according to the desired wavelength. The quantum harvesting efficiency of the spectrometer and CCD is about 55%. The fiber coupling efficiency is 60%. The loss efficiency of the beam splitting prism is 50%. Based on the above loss, the output SHG power and photon emission power were calculated. The excitation power was measured by an optical power meter (PM20CH,

Thorlabs). The energy conversion efficiency equals to the ratio of the original outgoing light power to the excitation power.

The two-dimensional photoluminescence spectrum was measured on a spectrometer (FL3-TCSPC, Horiba Jobin Yvon). The excitation light source was monitored at 5 nm intervals from 280 to 340 nm, and the photoluminescence signal was collected over a range of 350 to 650 nm. Ultraviolet-visible diffuse reflectance spectroscopy is measured on a spectrometer equipped with a diffuse integrating sphere attachment (UV-3600 Plus, Shimadzu). $BaSO_4$ is used as a reference. The slit width of the incident light is 2.00 nm.

Cyanobacterial strain and room-temperature fluorescence spectra

The cyanobacterial strain *Synechococcus sp.* PCC 7002 were cultured in media A supplemented with 0.01 M $NaNO_3$ (designated as A-plus media), bubbled with 1% CO_2. The growth temperature was 34ºC, and the light intensity was 250 μmol m^{-2} s^{-1} provided from cool-white fluorescent lights. The fluorescence spectrum of cyanobacteria upon different substrates (including chalcopyrite, glass, and galena) was measured using a Witec system (Alpha-700R) at room temperature, with an excitation wavelength of 1064 nm (pulse duration: 10 ps). The cyanobacteria were subjected to a 15-minute dark adaption before conducting fluorescence experiments.

Diamond anvil cell experiments

High-pressure SHG optical experiments were performed with the symmetric diamond anvil cells (DAC). Ultralow fluorescence diamonds with 400 μm culet was used. The sample chamber was defined by a hole with diameter of ~200 μm in a previously indented steel gasket. KBr and silicone oil were used as the pressure transmitting medium. The pressure of the sample environment was determined by the fluorescence emission of a ruby sphere loaded near the center of sample.

Metagenomic analysis

We downloaded 163 published metagenomics datasets (Supplementary Data1) to

analyze the existence of photosynthesis-related genes. The latitude and longitude information of datasets is included in Supplementary Data1. All photosynthesis-related genes were obtained from the KEGG Orthology database [72] to construct a photosynthetic gene database. The species information corresponding to the key photosynthetic genes is listed in Supplementary Data2. Metagenomic assemblies were generated using the MEGAHIT (v1.2.9) with default parameters [73]. The metagenomic reads from each dataset were mapped to this database using the DIAMOND BLASTx (v2.0.15.153) [74] to find the best hits. When multiple genes shared an alignment, the number of read hits were averaged. Metagenomic coverage values of photosynthesis-related genes were normalized using the number of metagenomic reads in each sample. Subsequently, a Perl script was used to calculated the maximum coverage for each gene and filter out results with coverage less than 80%. Based on the above results, we drew heatmaps using the Pheatmap R package (v 1.0.12) [75]. Some figures in this study were generated by the Generic Mapping Tools [76].

DATA AVAILABILITY

All data needed to evaluate the conclusions in the paper are present in the Supplementary Information. The raw metagenome reads utilized in this study have been made publicly accessible through their respective original publications as referenced in the Supplementary Table. The raw sequencing reads of the metatranscriptome have been deposited in the NCBI SRA (Sequence Read Archive) under the BioProject accession number PRJNA1133194.

SUPPLEMENTARY DATA

Supplementary Materials

This file contains Supplementary Figs. 1–13 and Supplementary methods.

Supplementary Data1

Supplementary Data2

ACKNOWLEDGEMENTS

We are grateful to the Institute of Deep Sea Science and Engineering, Chinese Academy of Sciences for generously providing the hydrothermal sulfide samples essential to this study. We extend our sincere appreciation to Prof. Huiming Bao for his invaluable suggestions on the original manuscript and his insightful discussions on the astrobiological implications of this work.

Finally, we thank the editor and anonymous reviewers for their constructive comments, which significantly improved the quality of this paper.

FUNDING

Y.L. acknowledges funding by the Natural Science Foundation of China (grant number 92351302, 42192502, 42372049). T.L. acknowledges funding by the Natural Science Foundation of China (grant number 92251304). A.L. acknowledges funding by the Natural Science Foundation of China (grant number 92251301). K.L. acknowledges funding by the National Key R&D Program of China (2022YFA1403504) and National Natural Science Foundation of China (52025023).

AUTHOR CONTRIBUTIONS

Y.L., J.D.Z., A.L. and T.L. conceived the project. T.L., Q.L., J.Q.Z., Y.L., H.N.J., H.Z.L., H.Y., and C.F.W. collected the metagenomics datasets, conducted metagenomics analysis, and cultured the cyanobacteria. K.H.L., Y.L., J.Q.Z., H.H., J.H.N., Y.Z.L. and X.J. constructed the optical set-up and conducted the spectroscopic measurements of minerals. J.Q.Z., H.Z.L., H.H. and J.X. conducted the fluorescence response experiments of cyanobacteria. B.X.H., J.Q.Z., Y.Z.L., H.H. and H.Z.L. constructed the diamond anvil cell (DAC) experiments. B.X.H. and J.Q.Z. conducted the density functional theory (DFT) calculations under pressure. Y.L., J.Q.Z., H.N.J., Q.L. and T.L. wrote the original manuscript. J.D.Z., H.H., Y.Z.L., K.H.L. and A.L. contributed to the revision of the paper.

REFERENCES

1. Dismukes G, Klimov V, Baranov S *et al.* The origin of atmospheric oxygen on Earth: the innovation of oxygenic photosynthesis. *Proc Natl Acad Sci*. 2001; **98**(5): 2170-2175.
2. Arndt NT, Nisbet EG. Processes on the young Earth and the habitats of early life. *Annu Rev Earth Planet Sci*. 2012; **40**: 521-549.
3. Gonnella G, Böhnke S, Indenbirken D *et al.* Endemic hydrothermal vent species identified in the open ocean seed bank. *Nat Microbiol*. 2016; **1**(8): 1-7.
4. Chen H, Li DH, Jiang AJ *et al.* Metagenomic analysis reveals wide distribution of phototrophic bacteria in hydrothermal vents on the ultraslow-spreading Southwest Indian Ridge. *Mar Life Sci Tech*. 2022; **4**(2): 255-267.
5. Puente-Sánchez F, Arce-Rodríguez A, Oggerin M *et al.* Viable cyanobacteria in the deep continental subsurface. *Proc Natl Acad Sci*. 2018; **115**(42): 10702-10707.
6. Cohen Y, Jørgensen BB, Revsbech NP *et al.* Adaptation to Hydrogen Sulfide of Oxygenic and Anoxygenic Photosynthesis among Cyanobacteria. *Appl Environ Microbiol*. 1986; **51**(2): 398-407.
7. Overmann J, Cypionka H, Pfennig N. An extremely low-light adapted phototrophic sulfur bacterium from the Black Sea. *Limnol Oceanogr*. 1992; **37**(1): 150-155.
8. Beatty JT, Overmann J, Lince MT *et al.* An obligately photosynthetic bacterial anaerobe from a deep-sea hydrothermal vent. *Proc Natl Acad Sci*. 2005; **102**(26): 9306-9310.
9. Holden JF, Breier JA, Rogers KL *et al.* Biogeochemical processes at hydrothermal vents:

microbes and minerals, bioenergetics, and carbon fluxes. *Oceanography*. 2012; **25**(1): 196-208.
10. Van Dover CL, Reynolds GT, Chave AD *et al.* Light at deep-sea hydrothermal vents. *Geophys Res Lett*. 1996; **23**(16): 2049-2052.
11. White SN. An investigation into the characteristics and sources of light emission at deep-sea hydrothermal vents. *Ph.D. Thesis. Type*. Massachusetts Institute of Technology, Department of Earth, Atmospheric, and Planetary Sciences, 2000.
12. White SN, Chave AD, Reynolds GT *et al.* Variations in ambient light emission from black smokers and flange pools on the Juan De Fuca Ridge. *Geophys Res Lett*. 2000; **27**(8): 1151-1154.
13. White SN, Chave AD, Reynolds GT. Investigations of ambient light emission at deep-sea hydrothermal vents. *J Geophys Res-Solid Earth*. 2002; **107**(B1): EPM 1-1-EPM 1-13.
14. White SN, Chave AD, Reynolds GT *et al.* Ambient light emission from hydrothermal vents on the Mid-Atlantic Ridge. *Geophys Res Lett*. 2002; **29**(15): 34-31-34-34.
15. Garten V, Head R. Crystalloluminescence and the nature of the critical nucleus. *Philos Mag*. 1963; **8**(95): 1793-1803.
16. Walton AJ. Triboluminescence. *Adv Phys*. 1977; **26**(6): 887-948.
17. Tapley DW, Buettner GR, Shick JM. Free radicals and chemiluminescence as products of the spontaneous oxidation of sulfide in seawater, and their biological implications. *Biol Bull*. 1999; **196**(1): 52-56.
18. Chakravarty A, Walton AJ. Light emission from collapsing superheated steam bubbles in water. *J Lumines*. 2000; **92**(1): 27-33.
19. Boyd RW. *Nonlinear Optics Second Edition*. California: Academic Press, 2003.
20. Atwood DA. *The rare earth elements: fundamentals and applications*. New Jersey: John Wiley & Sons, 2013.
21. Gaft M, Reisfeld R, Panczer G. *Modern luminescence spectroscopy of minerals and materials*. Switzerland: Springer, 2015.
22. Shen YR. *Principles of nonlinear optics*. New York: John Wiley & Sons, 1984.
23. Bu K, Fu T, Du Z *et al.* Enhanced second-harmonic generation of van der Waals $CuInP_2S_6$ via pressure-regulated cationic displacement. *Chem Mat*. 2022; **35**(1): 242-250.
24. Chen Q, Jian A, Li Z *et al.* Optofluidic tunable lenses using laser-induced thermal gradient. *Lab on a Chip*. 2016; **16**(1): 104-111.
25. Rockwell NC, Duanmu D, Martin SS *et al.* Eukaryotic algal phytochromes span the visible spectrum. *Proc Natl Acad Sci*. 2014; **111**(10): 3871-3876.
26. Baker NR, Oxborough K. Chlorophyll fluorescence as a probe of photosynthetic productivity. *Chlorophyll a fluorescence: a signature of photosynthesis*. Dordrecht: Springer, 2004: 65-82.
27. Murata N, Satoh K. Absorption and fluorescence emission by intact cells, chloroplasts, and chlorophyll-protein complexes. *Light emission by plants and bacteria*. 1986: 137-159.
28. Zhao J, Shen G, Bryant DA. Photosystem stoichiometry and state transitions in a mutant of the cyanobacterium *Synechococcus* sp. PCC 7002 lacking phycocyanin. *Biochimica et Biophysica Acta (BBA) - Bioenergetics*. 2001; **1505**(2): 248-257.
29. Brecht M, Nieder JB, Studier H *et al.* Red antenna states of photosystem I from *Synechococcus* sp. PCC 7002. *Photosynth Res*. 2008; **95**(2): 155-162.
30. Deng G, Liu F, Liu X *et al.* Significant energy transfer from CpcG2-phycobilisomes to

photosystem I in the cyanobacterium *Synechococcus* sp. PCC 7002 in the absence of ApcD-dependent state transitions. *FEBS Letters*. 2012; **586**(16): 2342-2345.
31. Watanabe M, Semchonok DA, Webber-Birungi MT *et al.* Attachment of phycobilisomes in an antenna–photosystem I supercomplex of cyanobacteria. *Proc Natl Acad Sci*. 2014; **111**(7): 2512-2517.
32. Hirose Y, Chihong S, Watanabe M *et al.* Diverse Chromatic Acclimation Processes Regulating Phycoerythrocyanin and Rod-Shaped Phycobilisome in Cyanobacteria. *Molecular Plant*. 2019; **12**(5): 715-725.
33. Allakhverdiev SI, Tsuchiya T, Watabe K *et al.* Redox potentials of primary electron acceptor quinone molecule $(QA)^-$ and conserved energetics of photosystem II in cyanobacteria with chlorophyll *a* and chlorophyll *d*. *Proc Natl Acad Sci*. 2011; **108**(19): 8054-8058.
34. Herzig PM, Hannington M. Polymetallic massive sulfides at the modern seafloor a review. *Ore Geol Rev*. 1995; **10**(2): 95-115.
35. Williams PA. *Oxide Zone Geochemistry*. New York: Ellis Horwood Ltd, 1990.
36. Pagliano C, Saracco G, Barber J. Structural, functional and auxiliary proteins of photosystem II. *Photosynth Res*. 2013; **116**: 167-188.
37. Sanfilippo JE, Garczarek L, Partensky F *et al.* Chromatic acclimation in cyanobacteria: a diverse and widespread process for optimizing photosynthesis. *Annu Rev Microbiol*. 2019; **73**(1): 407-433.
38. Ho M-Y, Gan F, Shen G *et al.* Far-red light photoacclimation (FaRLiP) in *Synechococcus* sp. PCC 7335. II.Characterization of phycobiliproteins produced during acclimation to far-red light. *Photosynth Res*. 2017; **131**(2): 187-202.
39. Soulier N, Laremore TN, Bryant DA. Characterization of cyanobacterial allophycocyanins absorbing far-red light. *Photosynth Res*. 2020; **145**(3): 189-207.
40. Bryant DA, Shen G, Turner GM *et al.* Far-red light allophycocyanin subunits play a role in chlorophyll *d* accumulation in far-red light. *Photosynth Res*. 2020; **143**(1): 81-95.
41. Partensky F, Hess WR, Vaulot D. *Prochlorococcus*, a Marine Photosynthetic Prokaryote of Global Significance. *Microbiol Mol Biol Rev*. 1999; **63**(1): 106-127.
42. Lin YS, Lin HT, Wang BS *et al.* Intense but variable autotrophic activity in a rapidly flushed shallow-water hydrothermal plume (Kueishantao Islet, Taiwan). *Geobiology*. 2021; **19**(1): 87-101.
43. Wang T-W, Lau DC, Chan T-Y *et al.* Autochthony and isotopic niches of benthic fauna at shallow-water hydrothermal vents. *Sci Rep*. 2022; **12**(1): 6248.
44. Hida S, Nishio M, Uesaka K *et al.* Microevolution toward loss of photosynthesis: Mutations promoting dark-heterotrophic growth and suppressing photosynthetic growth in cyanobacteria. *bioRxiv*. 2024: 2024.04.08.588626.
45. Hiraide Y, Oshima K, Fujisawa T *et al.* Loss of Cytochrome cM Stimulates Cyanobacterial Heterotrophic Growth in the Dark. *Plant Cell Physiol*. 2014; **56**(2): 334-345.
46. Baalen CV, Hoare DS, Brandt E. Heterotrophic Growth of Blue-Green Algae in Dim Light. *J Bacteriol*. 1971; **105**(3): 685-689.
47. Anderson SL, McIntosh L. Light-activated heterotrophic growth of the cyanobacterium *Synechocystis* sp. strain PCC 6803: a blue-light-requiring process. *J Bacteriol*. 1991; **173**(9): 2761-2767.
48. Stebegg R, Schmetterer G, Rompel A. Heterotrophy among Cyanobacteria. *ACS Omega*.

2023; **8**(37): 33098-33114.
49. Tell B, Kasper H. Optical and electrical properties of $AgGaS_2$ and $AgGASe_2$. *Phys Rev B*. 1971; **4**(12): 4455.
50. Medvedkin GA, Voevodin VG. Magnetic and optical phenomena in nonlinear optical crystals $ZnGeP_2$ and $CdGeP_2$. *J Opt Soc Am B*. 2005; **22**(9): 1884-1898.
51. You JW, Bongu SR, Bao Q *et al.* Nonlinear optical properties and applications of 2D materials: theoretical and experimental aspects. *Nanophotonics*. 2019; **8**(1): 63-97.
52. Zhou W, Guo S-P. Rational Design of Novel Promising Infrared Nonlinear Optical Materials: Structural Chemistry and Balanced Performances. *Accounts Chem Res*. 2024; **57**(4): 648-660.
53. Wintermans JFGM, De Mots A. Spectrophotometric characteristics of chlorophylls *a* and *b* and their phenophytins in ethanol. *Biochimica et Biophysica Acta (BBA) - Biophysics including Photosynthesis*. 1965; **109**(2): 448-453.
54. Zscheile F, White Jr JW, Beadle B *et al.* The preparation and absorption spectra of five pure carotenoid pigments. *Plant Physiol*. 1942; **17**(3): 331.
55. Six C, Thomas J-C, Garczarek L *et al.* Diversity and evolution of phycobilisomes in marine *Synechococcus* spp.: a comparative genomics study. *Genome Biol*. 2007; **8**: 1-22.
56. Bryant DA. Phycoerythrocyanin and phycoerythrin: properties and occurrence in cyanobacteria. *Microbiology*. 1982; **128**(4): 835-844.
57. Yücel M, Gartman A, Chan CS *et al.* Hydrothermal vents as a kinetically stable source of iron-sulphide-bearing nanoparticles to the ocean. *Nat Geosci*. 2011; **4**(6): 367-371.
58. Gartman A, Findlay AJ, Luther GW. Nanoparticulate pyrite and other nanoparticles are a widespread component of hydrothermal vent black smoker emissions. *Chem Geol*. 2014; **366**: 32-41.
59. Shi J, Wu X, Wu K *et al.* Giant Enhancement and Directional Second Harmonic Emission from Monolayer WS_2 on Silicon Substrate via Fabry-Pérot Micro-Cavity. *ACS Nano*. 2022; **16**(9): 13933-13941.
60. Kopp RE, Kirschvink JL, Hilburn IA *et al.* The Paleoproterozoic snowball Earth: a climate disaster triggered by the evolution of oxygenic photosynthesis. *Proc Natl Acad Sci*. 2005; **102**(32): 11131-11136.
61. Sánchez-Baracaldo P, Bianchini G, Wilson JD *et al.* Cyanobacteria and biogeochemical cycles through Earth history. *Trends Microbiol*. 2022; **30**(2): 143-157.
62. Aspler LB, Chiarenzelli JR. Two Neoarchean supercontinents? evidence from the Paleoproterozoic. *Sediment Geol*. 1998; **120**(1-4): 75-104.
63. Condie KC, Aster RC. Episodic zircon age spectra of orogenic granitoids: the supercontinent connection and continental growth. *Precambrian Res*. 2010; **180**(3-4): 227-236.
64. Anbar AD, Duan Y, Lyons TW *et al.* A whiff of oxygen before the great oxidation event? *Science*. 2007; **317**(5846): 1903-1906.
65. Turcotte D. On the thermal evolution of the Earth. *Earth Planet Sci Lett*. 1980; **48**(1): 53-58.
66. Mloszewska AM, Cole DB, Planavsky NJ *et al.* UV radiation limited the expansion of cyanobacteria in early marine photic environments. *Nat Commun*. 2018; **9**(1): 3088.
67. Sánchez-Baracaldo P, Raven JA, Pisani D *et al.* Early photosynthetic eukaryotes inhabited low-salinity habitats. *Proc Natl Acad Sci*. 2017; **114**(37): E7737-E7745.
68. Grettenberger C, Gold DA, Brown CT. Distribution of early-branching Cyanobacteriia and the potential habitats that gave rise to the earliest oxygenic phototrophs. *mSphere*. 2025;

10(2): e01013-01024.
69. Hoppe CJM, Fuchs N, Notz D *et al.* Photosynthetic light requirement near the theoretical minimum detected in Arctic microalgae. *Nat Commun*. 2024; **15**(1): 7385.
70. Lowell RP, DuBose M. Hydrothermal systems on Europa. *Geophys Res Lett*. 2005; **32**(5).
71. Hsu H-W, Postberg F, Sekine Y *et al.* Ongoing hydrothermal activities within Enceladus. *Nature*. 2015; **519**(7542): 207-210.
72. Kanehisa M. The KEGG database. In: *'In silico'simulation of biological processes: Novartis Foundation Symposium 247, 2002*, p. 91-103. Wiley Online Library.
73. Li D, Liu C-M, Luo R *et al*. MEGAHIT: an ultra-fast single-node solution for large and complex metagenomics assembly via succinct de Bruijn graph. *Bioinformatics*. 2015; **31**(10): 1674-1676.
74. Buchfink B, Reuter K, Drost H-G. Sensitive protein alignments at tree-of-life scale using DIAMOND. *Nat Methods*. 2021; **18**(4): 366-368.
75. Kolde R, Kolde MR. Package 'pheatmap'. *R package*. 2015; **1**(7): 790.
76. Wessel P, Luis JF, Uieda L *et al*. The Generic Mapping Tools Version 6. *Geochem. Geophys. Geosyst*. 2019; **20**(11): 5556-5564.